Production of heavy proton-rich nuclei and kinetic energy spectra of light nuclei in fusion-evaporation reactions*

Xiao-Jun Chen (陈晓君)[1] Xin-Yue Jia (贾欣玥)[1] Zi-Han Wang (王子涵)[1†]
Niu Wan (万牛)[1] Zhao-Qing Feng (冯兆庆)[1,2‡]

[1]School of Physics and Optoelectronics, South China University of Technology, Guangzhou 510640, China
[2]State Key Laboratory of Heavy Ion Science and Technology, Institute of Modern Physics, Chinese Academy of Sciences, Lanzhou 730000, China

Abstract: The fusion-evaporation excitation functions in the reactions of ^{12}C/^{16}O + ^{165}Ho, ^{12}C + ^{198}Pt/^{208}Pb/^{238}U, ^{16}O + ^{148}Sm/^{208}Pb/^{238}U, ^{20}Ne + ^{208}Pb/^{209}Bi, and ^{36,40}Ar + ^{182}W/^{185}Re/^{187}Os are systematically investigated using a combined approach of barrier distribution and statistical theory. The production cross sections of proton-rich nuclides $^{211-214}$U, $^{214-218}$Np, and $^{216-220}$Pu are estimated for the pure neutron and charged particle evaporation. The kinetic energy spectra of neutrons, protons, deuterons, tritons, and alphas from the compound nuclei in the fusion reactions are analyzed. We find that the Coulomb interaction between the charged particles and daughter nuclei dominates the kinetic energy spectra and leads to the Boltzmann distribution. The α yields are comparable with the hydrogen isotopes and are of the same order of magnitude. The shell effect is significant for fusion-evaporation cross sections and particle energy spectra.

Keywords: particle evaporation, kinetic energy spectra, fusion-evaporation reactions

DOI: 10.1088/1674-1137/ae37f1 **CSTR:** 32044.14.ChinesePhysicsC.50044112

I. INTRODUCTION

Over the past several decades, fusion reaction dynamics have been extensively investigated both through experiments and theories, particularly on the problems of "Big-Bang Nucleosynthesis," nuclear reactions in the stellar evolution, new isotope production, superheavy nucleus synthesis, and nuclear fission [1]. The fusion of heavy systems must overcome the Coulomb barrier formed by binary colliding nuclei and the competition between quasifission and complete fusion to form a compound nucleus. The synthesis of very heavy (superheavy) nuclei to reach the "island of stability" predicted theoretically and synthesizing new elements has progressed significantly through experiments on the fusion-evaporation reaction mechanism [2−7]. Superheavy nuclei (SHN) ($Z \geqslant 106$) exist owing to a strong shell effect against the large Coulomb repulsion. Fusion dynamics are associated with quantum tunneling through the coupling of relative motion and internal degrees of freedom. The initial configuration of colliding nuclei, nucleon or cluster transfer, deformation, shape evolution, *etc*., influence the formation of compound nuclei in the fusion reaction. In addition to the nuclear structure and proton-rich nuclide synthesis close to the drip line, the heavy-ion fusion reaction has been used to produce SHN, *i.e*., the well-known cold fusion reactions for element synthesis from Bh (Z=107) to Nh (Z=113) and the ^{48}Ca induced fusion reactions from Fl (Z=114) to Og (Z=118). The acccurate calculation of the fusion cross section in heavy-ion collisions is favorable for predicting the synthesis of new superheavy elements.

The compound nucleus formed in a fusion reaction is excited, and the de-excitation of the thermal nucleus proceeds via γ, neutron, and charged particle emissions against nuclear fission [8], in which the nuclear structure influences the de-excitation process, *i.e*., the level density, separation energy, fission barrier, shell effect, *etc*. The energy spectra of particles manifest the excited compound nucleus properties and are associated with the production of new isotopes in fusion reactions or multinucleon transfer reactions.

In this work, the production of heavy proton-rich nuclei and cluster kinetic energy spectra in fusion-evaporation reactions is systematically investigated within the framework of the dinuclear system (DNS) model. The remainder of this article is organized as follows. In Sec. II, we provide a brief description of the model. Calculated

Received 5 September 2025; Accepted 14 January 2026; Accepted manuscript online 15 January 2026
* Supported by the National Natural Science Foundation of China Projects (12575132, 12175072)
† E-mail: phwangzh@mail.scut.edu.cn
‡ E-mail: fengzhq@scut.edu.cn

results are discussed in Sec. III. A summary and perspective on the production of new proton-rich isotopes in experiments are presented in Sec. IV.

II. MODEL DESCRIPTION

In the work, the fusion-evaporation reactions with the charged particle channels and kinetic energy spectra are investigated systematically. It is well known that the evaporation residue cross section in fusion reactions is evaluated as a sum over partial angular momentum J at centre-of-mass energy $E_{\rm c.m.}$ in evaporation channel s:

$$\sigma^{s}_{ER}(E_{\rm c.m.}) = \frac{\pi\hbar^2}{2\mu E_{\rm c.m.}} \sum_{J=0}^{J_{\max}} (2J+1) T(E_{\rm c.m.}, J) \times P_{CN}(E_{\rm c.m.}, J) W^{s}_{\rm sur}(E_{\rm c.m.}, J) \quad (1)$$

Here, $T(E_{\rm c.m.})$ is the transmission probability of the two colliding nuclei overcoming the Coulomb barrier, which is calculated using the empirical coupled channel model [8, 9]. P_{CN} is the probability that the heavy system evolves from a touching configuration into the formation of compound nucleus in a competition of quasi-fission and fission of the heavy fragments.

The capture cross section of binary colliding system is given by

$$\sigma_{cap}(E_{\rm c.m.}) = \frac{\pi\hbar^2}{2\mu E_{\rm c.m.}} \sum_{J=0}^{J_{\max}} (2J+1) T(E_{\rm c.m.}, J), \quad (2)$$

where $T(E_{\rm c.m.}, J)$ is the penetration probability. For light and medium systems, $T(E_{\rm c.m.}, J)$ is calculated using the well-known Hill-Wheeler formula [10]:

$$T(E_{\rm c.m.}, J) = \int f(B) \frac{1}{1+\exp\left\{-\frac{2\pi}{\hbar\omega(J)}\left[E_{\rm c.m.} - B - \frac{J(J+1)\hbar^2}{2\mu R_B^2(J)}\right]\right\}} {\rm d}B, \quad (3)$$

with $\hbar\omega(J)$ being the width of the parabolic barrier at barrier radius $R_B(J)$ with the relation $R_B = r_{0b} * (A_P^{1/3} + A_T^{1/3})$, where $r_{0b} = 1.4 \sim 1.5$ fm.

The barrier distribution function is taken as the Gaussian form [8, 11]:

$$f(B) = \frac{1}{N} \exp[-((B - B_m)/\Delta)^2]. \quad (4)$$

The normalization constant satisfies $\int f(B){\rm d}B = 1$. The quantities B_m and Δ are evaluated using $B_m = (B_C + B_S)/2$ and $\Delta = (B_W - B_S)/2$, respectively. B_W is the Coulomb barrier at waist-to-waist orientation with static quadrupole deformation parameters β_P and β_T for projectile and target nuclei, respectively. B_S is the minimum barrier (barrier at saddle point) by varying the quadrupole deformation of the colliding partners. The nucleus-nucleus interaction potential with the dynamical quadrupole deformation is given by

$$V(\mathbf{R},\beta_P,\beta_T,\theta_P,\theta_T) = V_C(\mathbf{R},\beta_P,\beta_T,\theta_P,\theta_T) + V_N(\mathbf{R},\beta_P,\beta_T,\theta_P,\theta_T) + \frac{1}{2}C_P(\beta_P - \beta_P^0)^2 + + \frac{1}{2}C_T(\beta_T - \beta_T^0)^2. \quad (5)$$

Here, symbols P and T denote the projectile and target nuclei, respectively. $\mathbf{R}$ is the center-of-mass distance between the colliding partners. $\beta_{P,T}$ denotes the quadrupole deformation parameters corresponding to the minimum of $V(\mathbf{R},\beta_P,\beta_T,\theta_P,\theta_T))$, and $\beta^0_{P,T}$ denotes the parameters at the ground states for the projectile and target nuclei, respectively. The deformation energy is assumed to be proportional to the mass number, *i.e.*, $C_P\beta_P^2/C_T\beta_T^2 = A_P/A_T$, and stiffness parameter C_i (i=P,T) is calculated using the well-known liquid drop model as [12]

$$C_i = (\lambda - 1)\left[(\lambda - 1)R_i^2\sigma - \frac{3}{2\pi}\frac{Z_i^2 e^2}{R_i(2\lambda+1)}\right], \quad (6)$$

where R_{0i} is the spheroidal radius of the nucleus; its formula is $R_{0i} = 1.18A_i^{1/3}(i = 1, 2)$. Here, we consider only the quadrupole deformation ($\lambda = 2$). σ is the coefficient of surface tension that satisfies $4\pi R_i^2\sigma = a_s A_i^{2/3}$, and a_s = 18.32 MeV is the surface energy. The nuclear potential is calculated using the double-folding method based on the Skyrme interaction force neglecting the momentum and spin dependence [13]. The Coulomb potential is obtained using Wong's formula [14].

To describe the diffusion process along proton and neutron degrees of freedom in the competition of quasi-fission and complete fusion processes, we obtain the distribution probability by solving a set of master equations numerically on the potential energy surface of the DNS. The time evolution of the distribution probability $P(Z_1, N_1, E_1, t)$ for fragment 1 with proton number Z_1, neutron number N_1, and excitation energy E_1 is described using master equations as follows:

$$\frac{{\rm d}P(Z_1,N_1,E_1,t)}{{\rm d}t} = \sum_{Z_1'} W_{Z_1,N_1;Z_1',N_1}(t)[d_{Z_1,N_1}P(Z_1',N_1,E_1',t) - d_{Z_1',N_1}P(Z_1,N_1,E_1,t)] + \sum_{N_1'} W_{Z_1,N_1;Z_1,N_1'}(t)[d_{Z_1,N_1}P(Z_1,N_1',E_1',t) - d_{Z_1,N_1'}P(Z_1,N_1,E_1,t)] \quad (7)$$

Here, $W_{Z_1,N_1;Z_1',N_1}(W_{Z_1,N_1;Z_1,N_1'})$ is the mean transition probability from channel (Z_1,N_1,E_1) to (Z_1',N_1,E_1') [or from (Z_1,N_1,E_1) to (Z_1,N_1',E_1')], and d_{Z_1,Z_1} denotes the microscopic dimension corresponding to the macroscopic state (Z_1,N_1,E_1). The sum is taken over all possible proton and neutron numbers that fragment Z_1' and N_1' may take, but only one nucleon transfer is considered in the model with relations $Z_1' = Z_1 \pm 1$ and $N_1' = N_1 \pm 1$. Excitation energy E_1 is determined by the dissipation energy from the relative motion and potential energy surface of the DNS.

To form the compound nucleus, the DNS must overcome the inner fusion barrier. The fusion probability is estimated by integrating distribution probability $P(Z_1,N_1,E_1,t)$ to the Businaro-Gallone (BG) point. The formation probability of the compound nucleus at barrier B and angular momentum J is given by

$$P_{\rm CN}(E_{\rm c.m.},J) = \sum_{Z=1}^{Z_{\rm B.G.}}\sum_{N=1}^{N_{\rm B.G.}} P(Z_1,N_1,E_1,\tau_{\rm int}). \tag{8}$$

Here, interaction time $\tau_{\rm int}$ is obtained by using the deflection function method [8]. The fusion cross section is calculated by

$$\sigma_{\rm fus}(E_{\rm c.m.}) = \frac{\pi\hbar^2}{2\mu E_{\rm c.m.}}\sum_{J=0}^{J_{\max}}(2J+1)T(E_{\rm c.m.},J)\times P_{\rm CN}(E_{\rm c.m.},J). \tag{9}$$

However, for light reaction systems or projectile-target combinations with larger mass asymmetry ($A_P/A_T < 0.1$), the probability is close to unity, $P_{CN} \approx 1$, and fusion cross section $\sigma_{\rm fus}(E_{\rm c.m.}) \approx \sigma_{\rm cap}(E_{\rm c.m.})$ [15].

The compound nucleus formed in the fusion reactions is excited and is cooled via evaporating γ-rays, light particles (neutrons, protons, α, *etc*.) in competition with fission. The survival probability of the thermal nucleus in the channel of evaporating the $x-$th neutron, $y-$th proton, and $z-$th alpha is expressed by [16]

$$\begin{aligned} W_{\rm sur}(E^*_{\rm CN},x,y,z,J) =& P(E^*_{\rm CN},x,y,z,J) \\ &\times\prod_{i=1}^{x}\frac{\Gamma_n(E_i^*,J)}{\Gamma_{\rm tot}(E_i^*,J)}\prod_{j=1}^{y}\frac{\Gamma_p(E_j^*,J)}{\Gamma_{\rm tot}(E_j^*,J)} \\ &\times\prod_{k=1}^{z}\frac{\Gamma_\alpha(E_k^*,J)}{\Gamma_{\rm tot}(E_k^*,J)}. \end{aligned} \tag{10}$$

Here, $E^*_{\rm CN}$ and J are the excitation energy evaluated from the mass table in Ref. [17] and the spin of the excited nucleus, respectively. Total width $\Gamma_{\rm tot}$ is the sum of partial widths of particle evaporation, γ-emission, and fission. Excitation energy E_s^* before evaporating the s-th particle is evaluated as

$$E^*_{s+1} = E^*_s - B^n_i - B^p_j - B^\alpha_k - 2T_s \tag{11}$$

with the initial condition $E_1^* = E^*_{CN}$, and $s = i+j+k$. B^n_i, B^p_j, and B^α_k are the separation energies of the i-th neutron, j-th proton, and k-th alpha, respectively. Nuclear temperature T_i is given by $E_i^* = aT_i^2 - T_i$, where a is the level density parameter. The fission cross section of compound nucleus is estimated using

$$\begin{aligned} \sigma_{\rm fission}(E^*_{\rm CN}) =& \frac{\pi\hbar^2}{2\mu E_{\rm c.m.}}\sum_{J=0}^{J_{\max}}(2J+1)T(E_{\rm c.m.},J) \\ &\times P_{\rm CN}(E_{\rm c.m.},J)\frac{\Gamma_f(E^*_{\rm CN},J)}{\Gamma_{\rm tot}(E^*_{\rm CN},J)} \end{aligned} \tag{12}$$

with $E^*_{\rm CN} = E_{\rm c.m.} + Q_{PT}$ and fission width $\Gamma_f(E^*_{\rm CN},J)$, in which $\rm E_{c.m.}$ is the incident energy in the center-of-mass system. The reaction Q-value is estimated using $Q_{PT} = \triangle M_P + \triangle M_T - \triangle M_C$, where M_P, M_T, and M_C are the mass excesses for the projectile, target, and compound nuclei, respectively.

Assuming the electric dipole radiation (L=1) dominates $\gamma-$emission, the decay width is calculated using

$$\Gamma_\gamma(E^*_{\rm CN},J) = \frac{3}{\rho(E^*,J)}\int_{\varepsilon=0}^{E^*-\delta-\frac{1}{a}}\rho(E^*-E_{\rm rot}-\varepsilon,J)f_{E_1}(\varepsilon){\rm d}\varepsilon, \tag{13}$$

and

$$f_{E_1}(\varepsilon) = \frac{4}{3\pi}\frac{1+\kappa}{mc^2}\frac{e^2}{\hbar c}\frac{NZ}{A}\frac{\Gamma_G\varepsilon^4}{(\Gamma_G\varepsilon)^2+(\Gamma_G^2-\varepsilon^2)^2}. \tag{14}$$

Here, $\kappa = 0.75$, and Γ_G and E_G are the width and position of the electric dipole resonance, respectively. For a heavy nucleus, $\Gamma_G = 5$ MeV [18],

$$E_G = \frac{167.23}{A^{1/3}\sqrt{1.959+14.074A^{-1/3}}}{\rm MeV}. \tag{15}$$

The particle decay widths are evaluated using the Weisskopf evaporation theory as [19]

$$\begin{aligned} \Gamma_\nu(E^*,J) =& (2s_\nu+1)\frac{m_\nu}{\pi^2\hbar^2\rho(E^*,J)}\int_0^{E^*-B_\nu-\delta-\delta_n-\frac{1}{a}} \\ &\varepsilon\rho(E^*-B_\nu-\delta_n-E_{\rm rot}-\varepsilon,J)\sigma_{\rm inv}(\varepsilon){\rm d}\varepsilon. \end{aligned} \tag{16}$$

Here, s_ν, m_ν, and B_ν are the spin, mass, and binding energy of the evaporating particle, respectively. Pairing correction energy δ is set to $12/\sqrt{A}, 0, -12/\sqrt{A}$ MeV for even-even, even-odd, and odd-odd nuclei, respectively. The inverse cross section is given by $\sigma_{\rm inv} = \pi R_\nu^2 T(\nu)$. The penetration probability is set to unity for neutrons, and

$T(\nu) = (1+\exp(\pi(V_C(\nu)-\varepsilon)/\hbar\omega))^{-1}$ for charged particles, where $\hbar\omega = 5$ and 8 MeV for the proton and alpha, respectively. The fission width is calculated with a similar method as in Refs. [20, 21].

The level density is calculated from the Fermi-gas model as [22]

$$\rho(E^*,J) = K_{\rm coll}\cdot\frac{2J+1}{24\sqrt{2}\sigma^3 a^{1/4}(E^*-\delta)^{5/4}} \times\exp\left[2\sqrt{a(E^*-\delta)}-\frac{(J+1/2)^2}{2\sigma^2}\right], \quad (17)$$

with $\sigma^2 = 6\bar{m}^2\sqrt{a(E^*-\delta)}/\pi^2$ and $\bar{m}\approx 0.24A^{2/3}$. $K_{\rm coll}$ is the collective enhancement factor, which includes the rotational and vibrational effects [21, 23]. The level density parameter is related to shell correction energy $E_{\rm sh}(Z,N)$ and excitation energy E^* of the nucleus as

$$a(E^*,Z,N) = \tilde{a}(A)[1+E_{\rm sh}(Z,N)f(E^*-\Delta)/(E^*-\Delta)]. \quad (18)$$

Here, $\tilde{a}(A) = \alpha A+\beta A^{2/3}b_s$ is the asymptotic Fermi-gas value of the level density parameter at high excitation energies. The shell damping factor is given by

$$f(E^*) = 1-\exp(-\gamma E^*) \quad (19)$$

with $\gamma = \tilde{a}/(\epsilon A^{4/3})$ MeV^{-1}. Parameters α, β, b_s, and ϵ are taken to be 0.114, 0.098, 1., and 0.4, respectively [21]. The shell correction energy is taken from the mass table of the finite-range droplet model (FRDM2012) [24].

For one particle evaporation, the realization probability is given by

$$P(E^*_{\rm CN},J) = \exp\left(-\frac{(E^*_{\rm CN}-B_s-2T)^2}{2\sigma^2}\right). \quad (20)$$

Width σ is taken to fit the experimental width of fusion-evaporation excitation functions. Realization probability $P(E^*_{\rm CN},x,y,z,J)$ for evaporating x neutrons, y protons, z alphas at the excitation energy of $E^*_{\rm CN}$ and angular momentum of J is calculated using the Jackson formula [25] as

$$P(E^*_{\rm CN},s,J) = I(\Delta_s,2s-3)-I(\Delta_{s+1},2s-1), \quad (21)$$

where quantities I and Δ are given as follows:

$$I(z,m) = \frac{1}{m!}\int_0^z u^m {\rm e}^{-u}{\rm d}u, \quad (22)$$

$$\Delta_s = \frac{E^*_{CN}-\sum_{i=1}^{s}B_i^{\nu}}{T_i}. \quad (23)$$

B_i^{ν} is the separation energy of evaporating the i-th particle, and $s(x,y,z) = x+y+z$. The spectrum of the realization probability determines the structure of survival probability in each evaporation channel.

The kinetic energy of the charged particle evaporated from the compound nucleus is sampled using a Monte Carlo procedure within the energy range $\epsilon_\nu \in (0, E^*-B_\nu-V_C-E_{\rm rot})$. Here, V_C represents the Coulomb barrier between the charged particle and daughter nucleus. We neglect the quantum tunneling effect for penetrating the barrier at the low excitation energy. The Watt spectrum is used for the neutron emission [26] and is expressed as

$$\frac{{\rm d}\sigma_n}{{\rm d}\epsilon_n} = C_n\sigma_{\rm fus}(E_{\rm c.m.})\frac{\epsilon_n^{1/2}}{T_w^{3/2}}\exp\left(-\frac{\epsilon_n}{T_w}\right) \quad (24)$$

where $T_w = 1.7\pm0.1$ MeV, and C_n is the normalization constant. For the charged particles, the Boltzmann distribution is considered as [27, 28]

$$\frac{{\rm d}\sigma_\nu}{{\rm d}\epsilon_\nu} = 8\pi\sigma_{\rm fus}(E_{\rm c.m.})E_k\left(\frac{m}{2\pi T_\nu}\right)^{1/2}\exp\left(-\frac{\epsilon_\nu}{T_\nu}\right), \quad (25)$$

where $T_\nu = \sqrt{E^*/a}$, and $a = A/8$ MeV^{-1} is the level density parameter.

III. RESULTS AND DISCUSSION

Fusion-evaporation reactions have been extensively investigated for synthesizing new isotopes and extracting the structure effect in nuclear dynamics, *i.e.*, the cluster configuration, multidimensional coupling of nucleon transfer, deformation, collective rotation, *etc*. Charged particle evaporation is correlated with the excitation energy and nuclear structure of a compound nucleus. Fig. 1 shows is a comparison of fusion cross sections and evaporation residue (ER) excitation functions with the available experimental data in the reactions of ^{12}C + ^{165}Ho and ^{16}O + ^{165}Ho [29, 30]. For the reaction ^{12}C + ^{165}Ho, the pure neutron evaporation channels xn correspond to Ta isotope production. The channels of pxn and αxn evaporation are the Hf and Lu isotopes. Correspondingly, the Re, W, and Ta isotopes are produced via xn, pxn, and αxn evaporation in the reaction of ^{16}O + ^{165}Ho. The maximal evaporation cross sections in the 4-6n channels are close to those of the fusion cross section, in which the survival probabilities approach the unit. The $p3n$ and $p5n$ channels are two orders of magnitude lower than the experimental data for ^{173}Hf production with the cross section of 843±112 mb and ^{171}Hf with 145±22 mb [29]. The unexpected large experimental results are not explained by the model calculations. Typically, the ER cross sections with the charged particle channels are much lower than those of pure neutron evaporation because of the ex-

istence of Coulomb barrier. A similar case is observed in the reaction of ^{16}O + ^{165}Ho. Note that the cluster configuration of ^{12}C and ^{16}O is not considered in the present calculation of fusion ER excitation functions.

The fusion-evaporation residue excitation functions in the reactions of ^{16}O + ^{148}Sm, ^{16}O + ^{208}Pb, ^{12}C + ^{198}Pt, and ^{16}O + ^{238}U is calculated as shown in Fig. 2. The cross sections with the charged particles are lower by at least

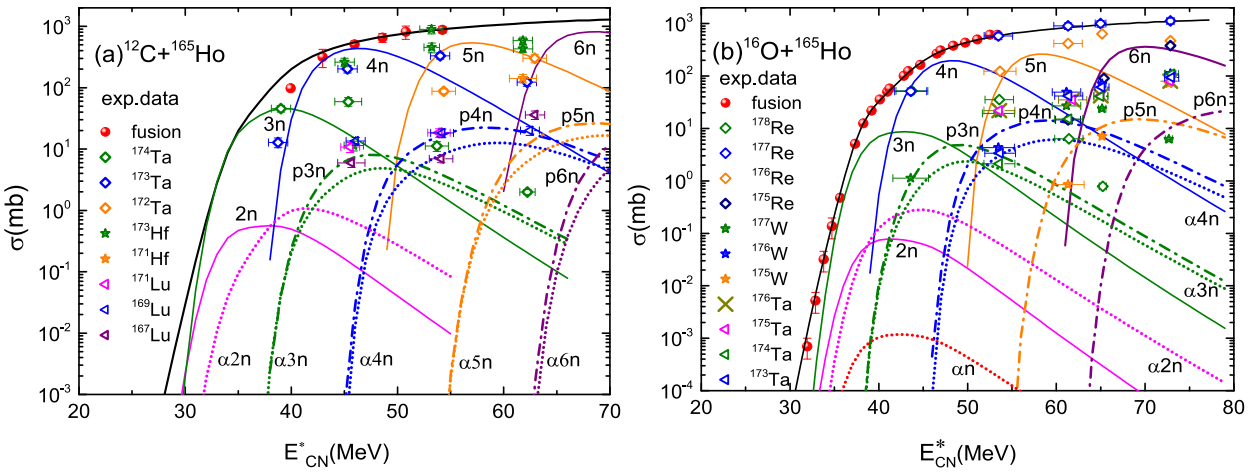

Fig. 1. (color online) Fusion and evaporation residue excitation functions in the reactions of (a) ^{12}C + ^{165}Ho and (b) ^{16}O + ^{165}Ho, respectively. The available experimental data are taken from Refs. [26, 27].

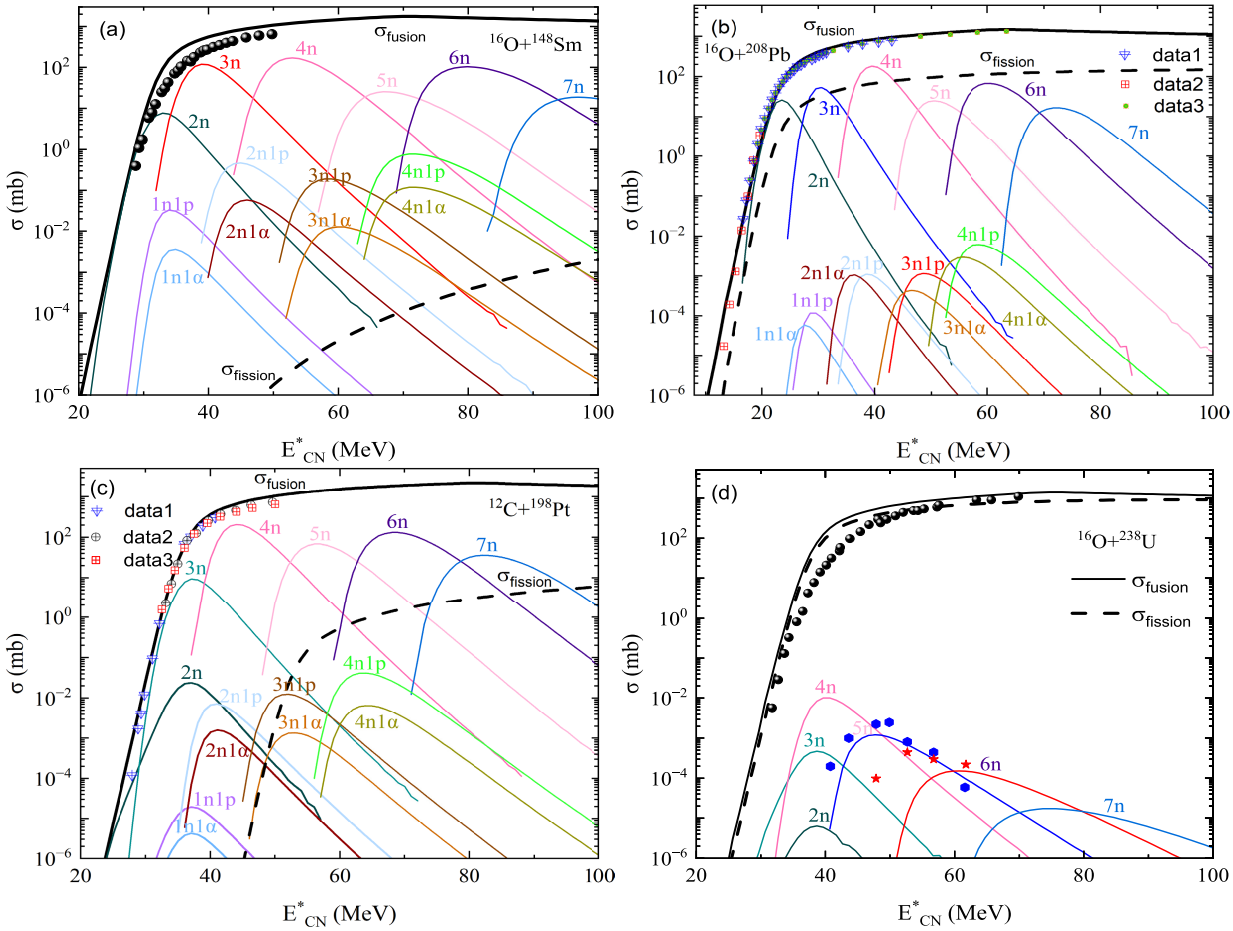

Fig. 2. (color online) Fusion and evaporation residue excitation functions in the reactions of (a) ^{16}O + ^{148}Sm, (b) ^{16}O + ^{208}Pb, (c) ^{12}C + ^{198}Pt, and (d) ^{16}O + ^{238}U, respectively. The experimental data are taken from Refs. [31−33].

two orders magnitude in comparison with those of pure neutron channels. The fission of the excited compound nucleus ^{254}Fm in the reaction ^{16}O + ^{238}U is dominant and leads to the reduction in ER cross sections. The fission cross section increases with the excitation energy and is apparent for the heavy compound nucleus formed in the fusion reaction. The ER cross sections with the charged particles are much lower than the pure neutron channels. The magnitude of reduction and the difference of *pxn* and *αxn* rely on the compound nuclei formed in the fusion reactions. The fusion-evaporation reactions for producing the actinide nuclei are influenced by the fission barrier, energy density, shell effect, *etc*. Fig. 3 shows the ER excitation functions in the *xn*, *xn*1α, and *xn*1*p* channels for the reactions ^{20}Ne + ^{208}Pb, ^{20}Ne + ^{209}Bi, ^{12}C + ^{208}Pb, and ^{12}C + ^{238}U, respectively. The optimal channel varies with the properties of compound nuclei in the pure neutron evaporation with the cross section from 0.1 mb (3n channel in ^{20}Ne + ^{209}Bi) to 300 mb (4n channel in ^{12}C + ^{208}Pb). The maximal cross section with the charged particle evaporation is rapidly reduced in comparison with the pure neutron evaporation, e.g., the five-order magnitude reduction from 4n to 3*n*1α (3*n*1*p*) channel in the reaction of ^{12}C + ^{208}Pb.

The production of new proton-rich actinide nuclides lays a foundation for investigating the decay mode and structure properties of nuclei close to the proton drip-line. The new magic number, fission barrier, decay mode, and level density deepen the understanding of SHN properties. ^{36,40}Ar induced fusion-evaporation reactions have been extensively performed to produce proton-rich nuclei around *N*=126 [34]. We analyzed the fusion-evaporation excitation functions for the pure neutron and charged particle channels in the reactions of ^{36,40}Ar + ^{182}W/^{185}Re/^{187}Os, as shown Fig. 4. The 2n-4n channels are dominant for producing the residue nuclei. The 5n-7n evaporation channels are available for new isotope production. Table 1 shows the production of new isotopes $^{211-214}$U, $^{214-218}$Np, and $^{216-220}$Pu in the fusion-evaporation reactions of ^{36}Ar + ^{182}W, ^{36}Ar + ^{185}Re, and ^{36}Ar + ^{187}Os, respectively. The production cross section, evaporation channel, excitation energy, and incident energy in the center-of-mass frame are shown for different systems. The cross section above nb is feasible in experiments and

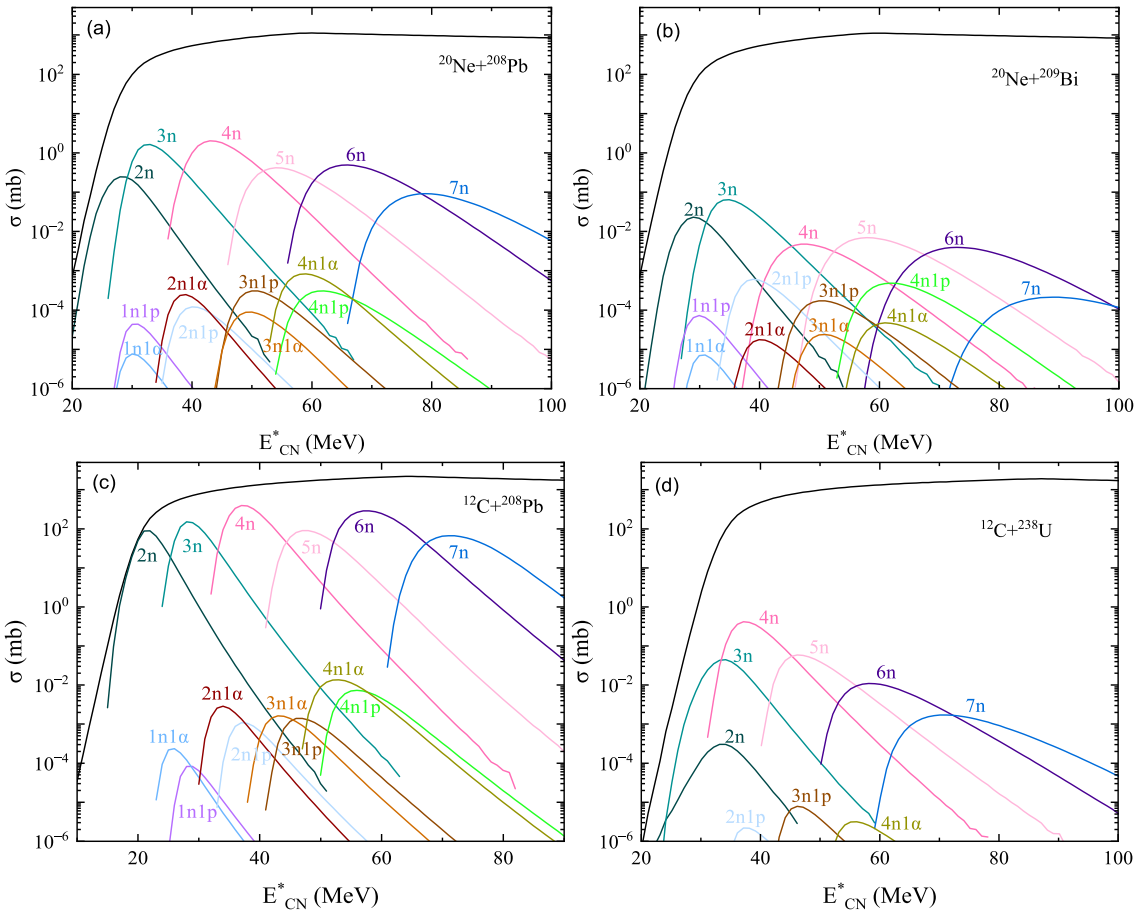

Fig. 3. (color online) Fusion and evaporation residue cross sections in the *xn*, *xn*1α, and *xn*1*p* chennels for the reactions (a) ^{20}Ne + ^{208}Pb, (b) ^{20}Ne + ^{209}Bi, (c) ^{12}C + ^{208}Pb, and (d) ^{12}C + ^{238}U, respectively.

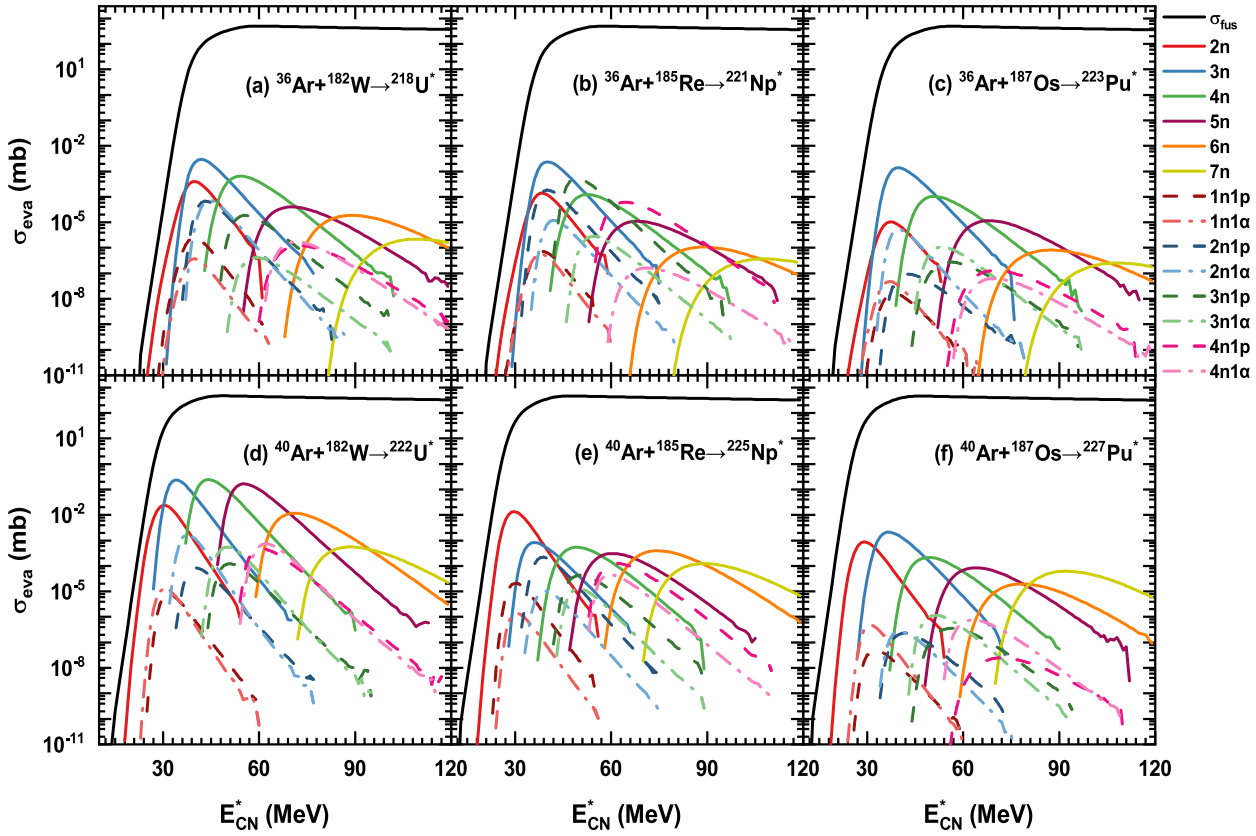

Fig. 4. (color online) Fusion-evaporation excitation functions for the pure neutron and charged particle channels in the reactions of ^{36,40}Ar + ^{182}W/^{185}Re/^{187}Os, respectively.

Table 1. Production of new isotopes $^{211-214}$U, $^{214-218}$Np, and $^{216-220}$Pu in the fusion-evaporation reactions of ^{36}Ar + ^{182}W, ^{36}Ar + ^{185}Re, and ^{36}Ar + ^{187}Os, respectively.

Reaction system	Reaction channel	Nuclide	Cross section	E^*_{CN}/MeV	$E_{\mathrm{c.m.}}$/MeV
^{36}Ar + ^{182}W	4n	^{214}U	0.65 μb	54	154.3
	5n	^{213}U	40.4 nb	70	170.3
	6n	^{212}U	18.8 nb	89	189.3
	7n	^{211}U	2.2 nb	109	209.3
^{36}Ar + ^{185}Re	3n	^{218}Np	2.36 μb	40	143.5
	4n	^{217}Np	124 nb	53	156.5
	5n	^{216}Np	11.1 nb	68	171.5
	6n	^{215}Np	1.1 nb	89	192.5
	7n	^{214}Np	0.37 nb	108	211.5
^{36}Ar + ^{187}Os	3n	^{220}Pu	1.37 μb	40	146.6
	4n	^{219}Pu	104 nb	51	157.6
	5n	^{218}Pu	11.6 nb	68	174.6
	6n	^{217}Pu	0.81 nb	87	193.6
	7n	^{216}Pu	0.25 nb	108	214.6

frequently identified by the cascade α-decay chain.

The kinetic energy spectra of particles manifest the excited properties of compound nuclei, *i.e.*, the rotational band, angular momentum, single particle energy, level density, fission barrier, *etc*. Fig. 5 shows the kinetic energy spectra of neutrons, protons, deuterons, tritons, and α from the compound nuclei formed in the reactions of ^{16}O + ^{208}Pb and ^{16}O + ^{238}U at an excitation energy of 42 MeV. The proton and α spectra are compared with the available experimental data and the GEMINI++ calculation. The solid lines in Fig. 5 (a) are the calculated results in this work. The energy spectra are primarily determined by the excitation energy of compound nucleus, separation energy of emitted cluster, and Coulomb barrier between the charged particle and daughter nucleus. The quantum tunneling is neglected in the calculation, which leads to the underestimation of low-energy particle production. The maximal position of charged particle energy spectra relies on the Coulomb energy. The hydrogen isotopes manifest a similar distribution because of the Coulomb interaction. We also compared the excitation energy dependence of neutrons, protons, deuterons, tritons, and α from the compound nuclei ^{210}Po and ^{214}Rn formed in collisions of ^{12}C+^{198}Pt and ^{16}O + ^{198}Pt, as shown in Fig. 6. A higher excitation energy leads to a broader energy tail. However, the maximal yields of the energy spectra are almost similar, *e.g.*, 10 MeV for the hydrogen isotopes and 20 MeV for α at the excitation energies of 61, 84, and 100 MeV, respectively. We observe that the energy spectra of deuterons are very close to those of tritons in the ^{12}C+^{198}Pt reaction but different for ^{16}O + ^{198}Pt, which is caused by the difference in cluster separation energies, *i.e.*, 10.22 and 10.85 MeV for deuteron and triton emissions from ^{210}Po, but 8.84 and 7.62 MeV for the deuteron and triton from ^{214}Rn. The system dependence of the cluster emission in the reactions of ^{12}C and ^{16}O on ^{208}Pb is calculated as shown in Fig. 7. The neutron emission is dominant with the lower kinetic energy in comparison with the hydrogen isotopes and α evaporation. The deuteron and triton energy spectra are similar in the reaction of ^{16}O + ^{208}Pb. The energetic cluster is produced by increasing the excitation energy of the compound nucleus. The higher Coulomb barrier enables the particle emission to the high-energy tail.

The energy spectra of cluster emission in massive transfer and fusion reactions are sensitive probes for extracting the nuclear structure and reaction dynamics of the intermediate stage. The cluster evaporation from the compound nucleus is correlated with the excited sate, excitation energy, angular momentum, cluster configuration, separation energy, *etc*. Fig. 8 shows a comparison of the kinetic energy spectra of neutrons, protons, deuterons, tritons, and alphas from the compound nuclei formed in the reactions of ^{12}C+^{238}U (upper panel) and ^{16}O+^{238}U (down panel) at the excitation energies of 61, 84, and 100 MeV, respectively. The nuclear fission is dominant in the formation of a compound nucleus in comparison with the fusion-evaporation reaction. The charged particle yields are significantly reduced in comparison with the neutron emission. The mixed channels of the charged particle and neutron evaporation are available for the new isotope production. The evaporation channels with proton and α emission should be considered in the synthesis of SHN.

IV. CONCLUSIONS

Fusion-evaporation reactions for producing the proton-rich nuclei around N=126 have been extensively in-

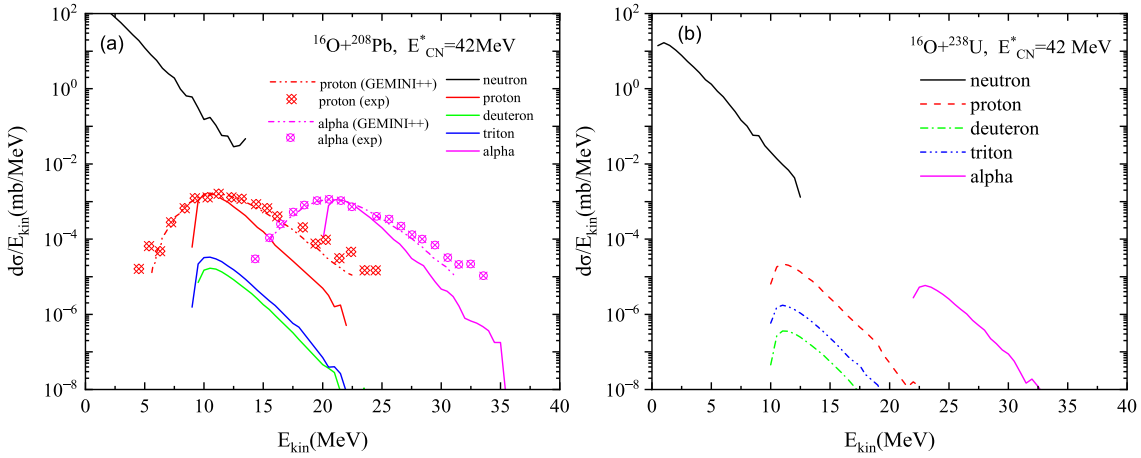

Fig. 5. (color online) Kinetic energy spectra of neutrons, protons, deuterons, tritons, and alphas from the compound nuclei formed in the reactions of (a) ^{16}O+^{208}Pb and (b) ^{16}O+^{238}U at the excitation energy 42 MeV of compound nuclei. The available experimental data [35] and results of GEMINI++, indicated by dash-dotted lines [36], are shown for comparison with the results in this work for ^{16}O+^{208}Pb (left panel), indicated by solid lines.

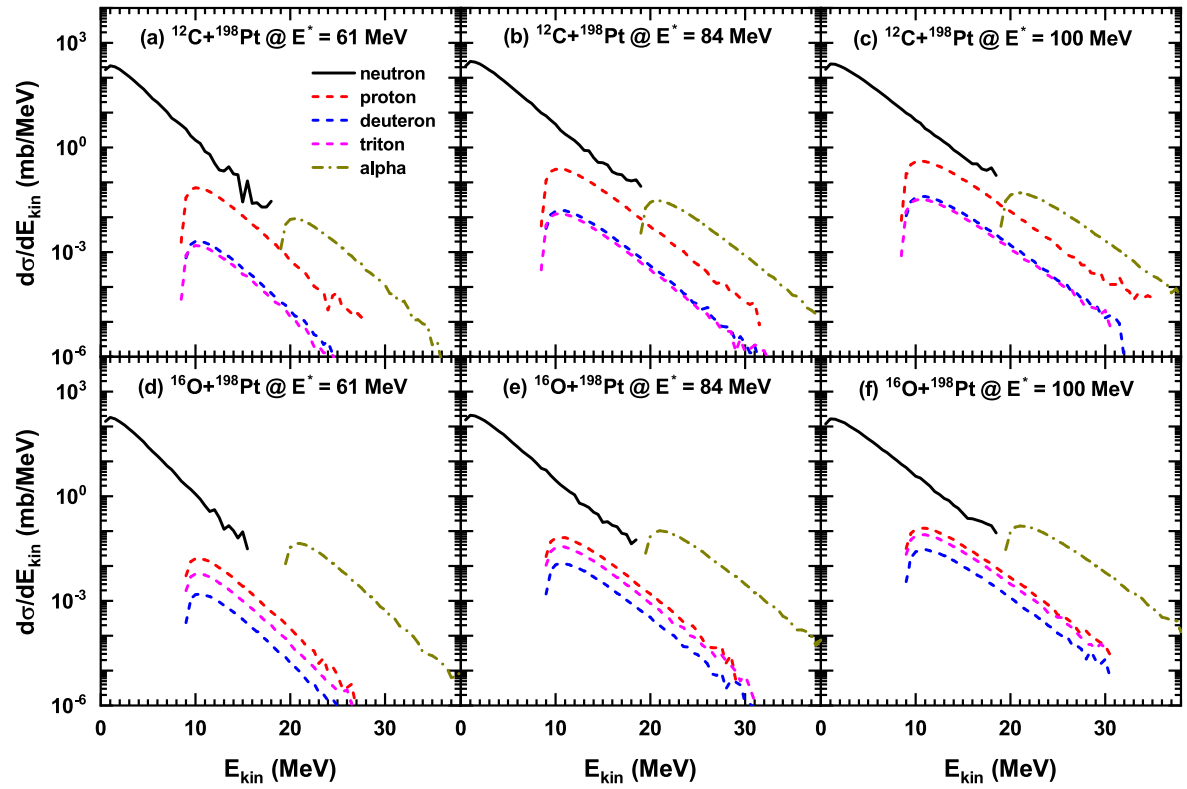

Fig. 6. (color online) Kinetic energy spectra of neutrons, protons, deuterons, tritons, and alphas from the compound nuclei ^{210}Po and ^{214}Rn in the reactions of (a) ^{12}C+^{198}Pt and (b) ^{16}O+^{198}Pt at excitation energies of 61, 84, and 100 MeV, respectively.

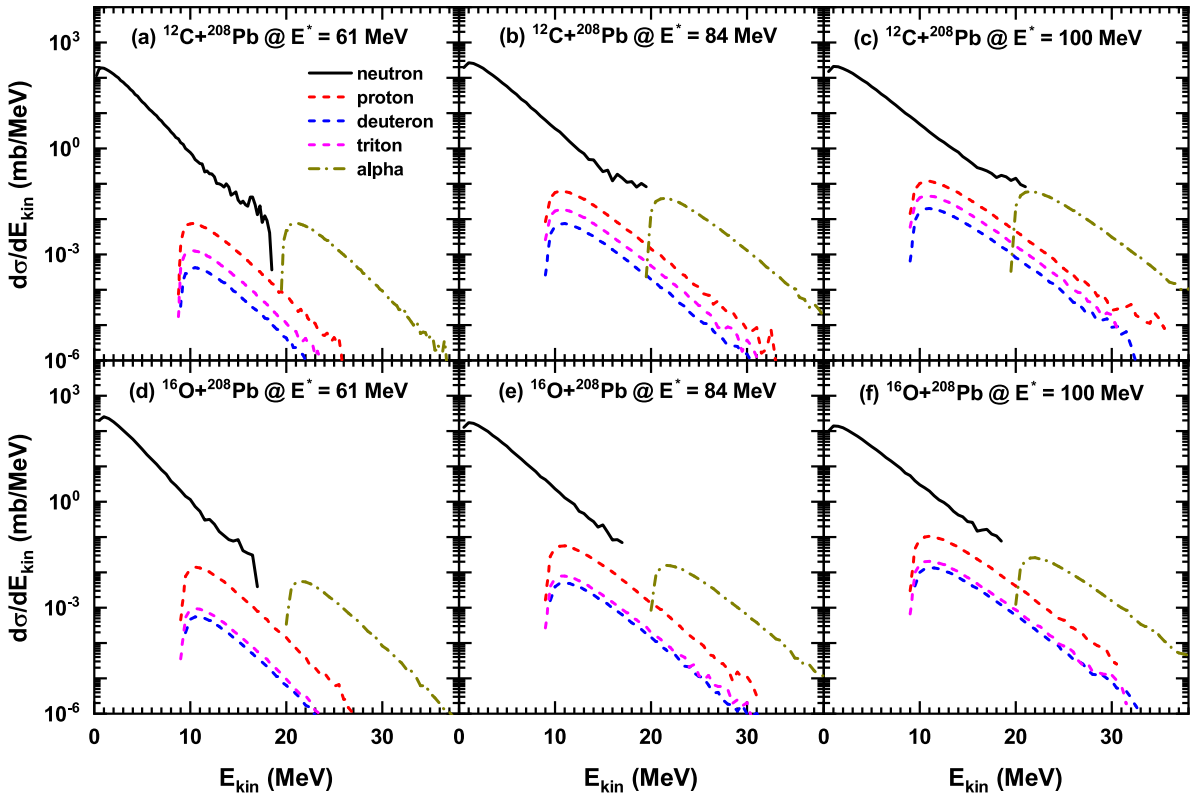

Fig. 7. (color online) Same as in Fig. 6, but for the deexcitation of ^{220}Ra and ^{224}Th in the reactions of ^{12}C and ^{16}O on ^{208}Pb.

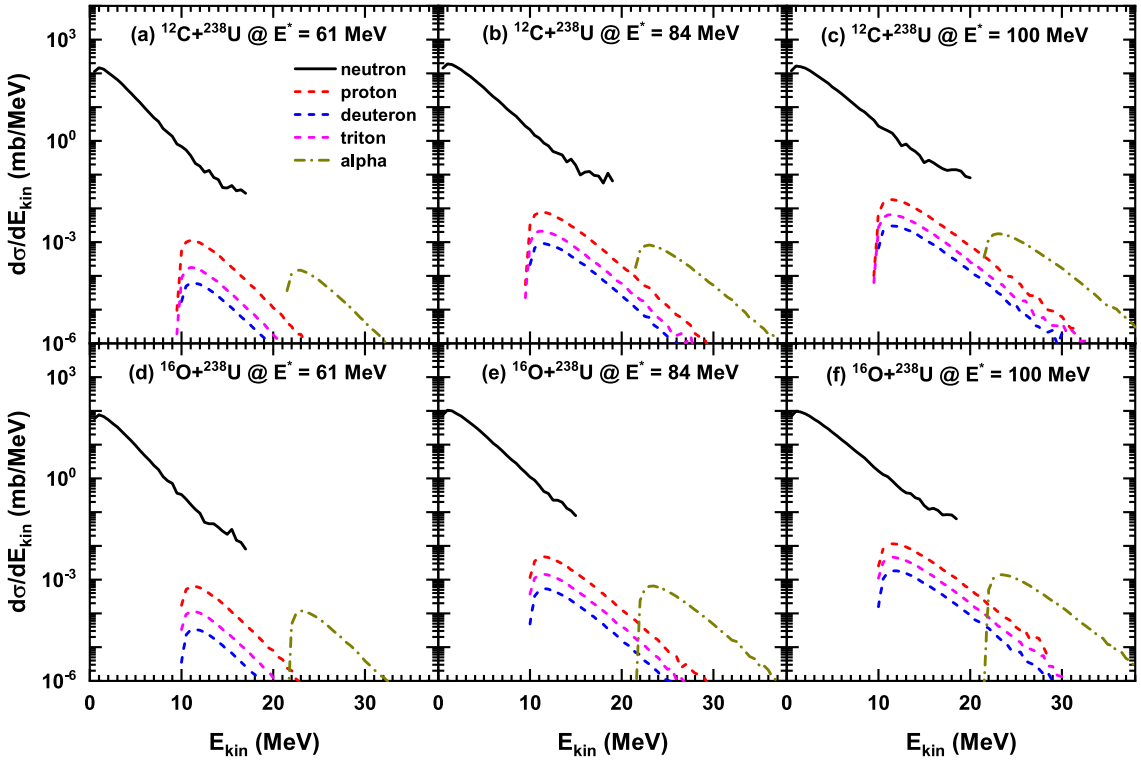

Fig. 8. (color online) Kinetic energy spectra of neutrons, protons, deuterons, tritons, and alphas produced in the fusion-evaporation reactions of ^{12}C and ^{16}O on ^{238}U.

vestigated. The cross sections of pure neutron and mixed evaporation channels with charged particles are systematically calculated using the dinuclear system model. The production of new proton-rich isotopes $^{211-214}$U, $^{214-218}$Np, and $^{216-220}$Pu with the cross sections of 0.25 nb−2.36 μb is analyzed via the reactions of ^{36}Ar + ^{182}W/^{185}Re/^{187}Os. The systems are feasible in experiments, and the decay modes of the new isotopes are still of interest in nuclear structure studies. The kinetic energy spectra of neutrons, protons, deuterons, tritons, and α from compound nuclei strongly depend on the excitation energy and Coulomb interaction between the charged particles and daughter nuclei. The shell effect of compound nuclei in the fusion reactions influences the α yields and energy spectra.

References

[1] B. B. Back, H. Esbensen, C. L. Jiang *et al.*, Rev. Mod. Phys. **86**, 317 (2014)
[2] S. Hofmann and G. Münzenberg, Rev. Mod. Phys. **72**, 733 (2000)
[3] G. Münzenberg, Nucl. Phys. A **944**, 5 (2015)
[4] K. Morita, K. Morimoto, D. Kaji *et al.*, J. Phys. Soc. Jpn. **73**, 2593 (2004)
[5] K. Morita, Nucl. Phys. A **944**, 30 (2015)
[6] Y. Oganessian, J. Phys. G: Nucl. Part. Phys. **34**, R165 (2007)
[7] Y. Oganessian and V. K. Utyonkov, Nucl. Phys. A **944**, 62 (2015)
[8] Z. Q. Feng, G. M. Jin, F. Fu *et al.*, Nucl. Phys. A **771**, 50 (2006)
[9] V. I. Zagrebaev, Phys. Rev. C **67**, 061601 (R) (2003)
[10] D. L. Hill and J. A. Wheeler, Phys. Rep. **89**, 1102 (1953)
[11] V. I. Zagrebaev, Y. Aritomo, M. G. Itkis *et al.*, Phys. Rev. C **65**, 014607 (2001)
[12] W. D. Myers and W. J. Swiatecki, Nucl. Phys. **81**, 1 (1966)
[13] G. G. Adamian, N. V. Antonenko, R. Jolos *et al.*, Int. J. Mod. Phys. E **5**, 191 (1996)
[14] C. Y. Wong, Phys. Rev. Lett. **31**, 766 (1973)
[15] R. Yanez *et al.*, Phys. Rev. C **88**, 014606 (2013)
[16] P. H. Chen, Z. Q. Feng, J. Q. Li *et al.*, Chin. Phys. C **40**, 091002 (2016)
[17] P. Möller *et al.*, At. Data Nucl. Data Tables **59**, 185 (1995)
[18] K. H. Schmidt and W. Morawek, Rep. Prog. Phys. **54**, 949 (1991)
[19] V. Weisskopf, Phys. Rev. **52**, 295 (1937)
[20] Z. Q. Feng, G. M. Jin, J. Q. Li *et al.*, Phys. Rev. C **76**, 044606 (2007)
[21] Z. Q. Feng, G. M. Jin, and J. Q. Li, Nucl. Phys. A **816**, 33 (2009)
[22] A. V. Ignatyuk, K. K. Istekov, and G. N. Smirenkin, Nucl. Phys. **29**, 875 (1979)
[23] A. R. Junghans, M. de Jong, H. G. Clerc *et al.*, Nucl. Phys. A **629**, 635 (1998)
[24] P. Möller, A. J. Sierk, T. Ichikawa *et al.*, Atomic Data and

Nuclear Data Tables **109-110**, 1 (2016)
[25] J. D. Jackson, Can. J. Phys. **34**, 767 (1956)
[26] H. Rossner, Phys. Rev. C **45**, 719 (1992)
[27] Z. Q. Feng, Phys. Rev. C **107**, 054613 (2023)
[28] Z. H. Wang, Y. L. Zhang, and Z. Q. Feng, Nucl. Sci. Tech. **36**, 229 (2025)
[29] S. Gupta, B. P. Singh, M. M. Musthafa *et al*., Phys. Rev. C **61**, 064613 (2000)
[30] K. Kumar, T. Ahmad, S. Ali *et al*., Phys. Rev. C **87**, 044608 (2013)
[31] E. V. Prokhorova, A. A. Bogachev, M. G. Itkis *et al*., Nucl. Phys. A **802**, 45 (2008)
[32] M. Dasgupta and D. J. Hinde, Nucl. Phys. A **734**, 148 (2004)
[33] K. Nishio, H. Ikezoe, Y. Nagame *et al*., Phys. Rev. Lett. **93**, 162701 (2004)
[34] H. B. Yang, L. Ma, Z. Y. Zhang *et al*., Phys. Rev. C **91**, 051302 (2015)
[35] B. J. Fineman, K. T. Brinkmann, A. L. Caraley *et al*., Phys. Rev. C **50**, 1991 (1994)
[36] R. J. Charity, Phys. Rev. C **82**, 014610 (2010)